PAPER

Self-assembled fibrillar networks of a multifaceted chiral squaramide: supramolecular multistimuli-responsive alcogels†

Jana Schiller,[a] Juan V. Alegre-Requena,[ab] Eugenia Marqués-López,[b] Raquel P. Herrera,[b] Jordi Casanovas,[c] Carlos Alemán[d] and David Díaz Díaz*[ae]

Chiral N,N′-disubstituted squaramide **1** has been found to undergo self-assembly in a variety of alcoholic solvents at low concentrations leading to the formation of novel nanostructured supramolecular alcogels. The gels responded to thermal, mechanical, optical and chemical stimuli. Solubility studies, gelation ability tests and computer modeling of a series of structurally related squaramides proved the existence of a unique combination of non-covalent molecular interactions and favorable hydrophobic/hydrophilic balance in **1** that drive the anisotropic growth of alcogel networks. The results have also revealed a remarkable effect of ultrasound on both the gelation kinetics and the properties of the alcogels.

Introduction

Squaramides are four-membered vinylogously conjugated diamides derived from squaric acid and possess a very high synthetic versatility.[1] Overall, the field of squaramides has experienced an extraordinary growth since the pioneering study of Rawal and co-workers[2] using these compounds as organocatalysts. Moreover, squaramides have been recognized as bioisosteres of ureas[3] exhibiting appealing properties for diverse research areas beyond organocatalysis,[4–6] such as biomedicine,[1] synthesis[7] and crystal engineering.[8–12] One of the most important features of these scaffolds is their capacity for selectively binding to different hydrogen bond acceptors through their acidic NH groups. Remarkably, squaramides play a dual role as they are also able to act as good hydrogen bond acceptors, making them suitable as receptors for cation recognition. This property has been explored to find promising candidates for the development

of novel drugs[1,13,14] and in the field of organocatalysis as chiral hydrogen bond donor catalysts.[4] However, despite the increasing number of squaramide-based compounds in the literature, the study of their self-assembly properties in solution for the synthesis of soft functional materials has remained virtually unexplored.[15]

Within this context, hierarchical gel-based materials have received increasing attention over the last decades[16–27] due to their unique architectures and potential for high-tech applications in numerous fields including, among others,[28–32] the fabrication of sensors,[33] liquid crystals,[34] electrically conductive scaffolds,[35,36] templates for the growth of cells and inorganic structures,[37,38] chemical catalysis,[39] as well as in cosmetic and food industries.[16] In contrast to chemical gels[40–42] that are based on covalent bonds, (*e.g.*, cross-linked polymers), physical gels[1,43–50] are typically made of low molecular weight compounds self-assembled through non-covalent interactions (*e.g.*, hydrogen-bonding, van der Waals, charge-transfer, dipole–dipole, π–π stacking and coordination interactions), which usually provides reversible gel-to-sol phase transitions as response to environmental stimuli.[51,52] Systems based on both types of connections are also known.[53,54] The solid-like appearance and rheological properties of the gels result from the immobilization of the liquid (major component) into the interstices of a solid matrix (minor component) through capillary forces.[51,55] The formation of the 3D-network with numerous junction zones[56,57] is a consequence of the entanglement of 1D-polymeric strands of gelator molecules[16] typically of nm diameters and μm lengths.[58,59]

Herein, we report the unprecedented self-assembly properties of a chiral squaramide in numerous alcoholic solvents leading to the formation of multistimuli-responsive supramolecular alcogels. The remarkable effect of ultrasound during the preparation

[a] *Institut für Organische Chemie, Universität Regensburg, Universitätsstr. 31, 93053 Regensburg, Germany. E-mail: David.Diaz@chemie.uni-regensburg.de; Fax: +49 941 9434121; Tel: +49 941 9434373*

[b] *Laboratorio de Organocatálisis Asimétrica, Departamento de Química Orgánica, Instituto de Síntesis Química y Catálisis Homogénea (ISQCH), CSIC-Universidad de Zaragoza, Pedro Cerbuna 12, 50009 Zaragoza, Spain*

[c] *Departament de Química, EPS, Universitat de Lleida, Jaume II 69, 25001 Lleida, Spain*

[d] *Departament d'Enginyeria Química – ETSEIB and Center for Research in Nano-Engineering, Universitat Politècnica de Catalunya, Av. Diagonal 647, 08028 Barcelona, Spain*

[e] *IQAC-CSIC, Jordi Girona 18-26, 08034 Barcelona, Spain*

† Electronic supplementary information (ESI) available: Spectroscopy, rheology, additional experimental and calculation details, pictures and tables. See DOI: 10.1039/c5sm02997j

of the gels as well as the plausible gelation mechanism supported by quantum mechanical calculations are also discussed. This work expands the applications of squaramides towards materials synthesis.

Experimental

(A) Synthesis and characterization of compounds

Materials. Unless otherwise noted, all solvents and reagents were purchased from commercial suppliers and used as received.

Characterization methods. Purification of reaction products was carried out by filtration. Analytical thin layer chromatography was performed on 0.25 mm silica gel 60-F plates. ESI ionization method and mass analyzer type MicroTof-Q were used for the MS measurements. ^{1}H-NMR spectra were recorded at 400 MHz and ^{13}C-NMR-APT spectra were recorded at 100 MHz, using DMSO-d_6 as deuterated solvent. Chemical shifts were reported in the δ scale relative to residual DMSO (2.50 ppm for ^{1}H-NMR and 39.43 ppm for ^{13}C-NMR-APT). The ^{1}H-NMR and ^{13}C-NMR spectra of compounds **1**,[60] **2**,[61] **3**,[62] **4**,[60] **7**,[60] **8**,[60] and **9**[60] were consistent with those previously reported in the literature.

General procedure for the synthesis of compounds 5, 6 and 10. To a solution of 3,4-dimethoxy-3-cyclobutene-1,2-dione (**11**) (1.2 or 3 mmol) in MeOH (3–3.75 mL), amine **12** (1.2 or 3 mmol) was added at room temperature. After the corresponding reaction time (t_1), amine **13** (1.2 or 3 mmol) was then added dissolved in MeOH (9 or 11.25 mL). After the corresponding reaction time (t_2), the reaction flask was placed in the freezer (−20 °C) for 30 minutes and the obtained product was purified by filtration. See ESI† (Scheme S1) for exact solvent volumes and reaction times in each case.

3-(((1S,2R)-2-Hydroxy-2,3-dihydro-1H-inden-1-yl)amino)-4-(phenylamino)cyclobut-3-ene-1,2-dione (5). Following the above general procedure using 3 mmol of **11**, compound **5** was obtained after 9 h of reaction at room temperature as a white solid in 86% yield. Mp 248–250 °C Decomp. $[\alpha]_D^{30}$ = +39.6° (c 0.61, DMSO). ^{1}H-NMR (300 MHz, DMSO-d_6) δ 9.90 (br s, 1H), 8.07 (d, J = 9.1 Hz, 1H), 7.49 (d, J = 7.8 Hz, 2H), 7.42–7.21 (m, 6H), 7.07–6.96 (m, 1H), 5.54 (br s, 1H), 5.54 (dd, J = 8.8, 5.0 Hz, 1H), 4.58 (dt, J = 4.9, 1.6 Hz, 1H), 3.14 (dd, J = 15.7, 4.4 Hz, 1H), 2.88 (dd, J = 16.3, 1.4 Hz, 1H). ^{13}C-NMR-APT (75 MHz, DMSO-d_6) δ 183.9 (1C), 180.3 (1C), 169.0 (1C), 163.7 (1C), 141.3 (1C), 140.5 (1C), 139.1 (1C), 129.2 (2C), 127.9 (1C), 126.6 (1C), 125.0 (1C), 124.2 (1C), 122.4 (1C), 117.8 (2C), 72.3 (1C), 61.1 (1C), 39.3 (1C). IR (KBr film) (cm^{-1}) ν 3426, 3283, 2923, 2853, 1797, 1661, 1606, 1567, 1543, 1455, 1423, 1377, 1092, 760, 751, 744, 430. MS (ESI+) 343.1 [M + Na]. HRMS (ESI+) calcd for $C_{19}H_{16}N_2NaO_3$ 343.1053; found 343.1046 [M + Na].

3-(((1S,2R)-2-Hydroxy-2,3-dihydro-1H-inden-1-yl)amino)-4-((4-methoxyphenyl)amino)cyclobut-3-ene-1,2-dione (6). Following the above general procedure using 3 mmol of **11**, compound **6** was obtained after 10 h of reaction at room temperature as a white solid in 88% yield. Mp 254–256 °C Decomp. $[\alpha]_D^{29}$ = +41.8° (c 0.60, DMSO). ^{1}H-NMR (300 MHz, DMSO-d_6) δ 9.80 (s, 1H),

8.07 (br d, J = 8.9 Hz, 1H), 7.41 (d, J = 8.9 Hz, 2H), 7.46–7.19 (m, 4H), 6.93 (d, J = 9.0 Hz, 2H), 5.55 (br s, 1H), 5.53 (dd, J = 9.0, 4.8 Hz, 1H), 4.57 (dt, J = 4.8, 1.6 Hz, 1H), 3.73 (s, 3H), 3.14 (dd, J = 16.3, 4.9 Hz, 1H), 2.87 (dd, J = 16.5, 1.3 Hz, 1H). ^{13}C-NMR-APT (75 MHz, DMSO-d_6) δ 183.3 (1C), 180.4 (1C), 168.6 (1C), 163.7 (1C), 155.1 (1C), 141.4 (1C), 140.5 (1C), 132.3 (1C), 127.9 (1C), 126.5 (1C), 125.0 (1C), 124.2 (1C), 119.3 (2C), 114.5 (2C), 72.3 (1C), 61.1 (1C), 55.2 (1C), 39.3 (1C). IR (KBr film) (cm^{-1}) ν 3413, 3278, 2923, 2853, 1795, 1656, 1605, 1565, 1541, 1517, 1496, 1459, 1426, 1419, 1377, 1351, 1321, 1257, 1209, 1183, 1157, 1140, 1116, 1099, 1032, 1001, 872, 861, 801, 773, 747, 637, 599, 439. MS (ESI+) 373.2 [M + Na]. HRMS (ESI+) calcd for $C_{20}H_{18}N_2NaO_4$ 373.1159; found 373.1151 [M + Na].

***N*-((1R,2R)-2-((2-(Hexylamino)-3,4-dioxocyclobut-1-en-1-yl)amino)-cyclohexyl)-4-methylbenzenesulfonamide (10).** Following the above general procedure using 1.2 mmol of **11**, compound **10** was obtained after 5 h of reaction at room temperature as a white solid in 74% yield. Mp 210–212 °C. $[\alpha]_D^{30}$ = +18.2° (c 0.64, DMSO). ^{1}H-NMR (300 MHz, DMSO-d_6) δ 7.61 (d, J = 8.2 Hz, 2H), 7.54 (d, J = 7.7 Hz, 1H), 7.32 (br s, 1H), 7.29 (d, J = 8.1 Hz, 2H), 7.18 (d, J = 7.9 Hz, 1H), 3.60–3.36 (m, 3H), 3.12–2.96 (m, 1H), 2.36 (s, 3H), 1.92–1.78 (m, 1H), 1.66–1.00 (m, 14H), 0.96–0.77 (m, 4H). ^{13}C-NMR-APT (75 MHz, DMSO-d_6) δ 182.0 (1C), 181.8 (1C), 167.7 (1C), 167.2 (1C), 142.0 (1C), 139.3 (1C), 129.2 (2C), 125.9 (2C), 56.8 (1C), 56.4 (1C), 43.1 (1C), 33.0 (1C), 32.5 (1C), 30.7 (1C), 30.5 (1C), 25.4 (1C), 24.0 (2C), 21.9 (1C), 20.8 (1C), 13.8 (1C). IR (KBr film) (cm^{-1}) ν 3197, 2956, 2923, 28 569, 1798, 1656, 1650, 1572, 1521, 1465, 1342, 1162, 1094, 814, 665, 575, 549, 419. MS (ESI+) 470.3 [M + Na]. HRMS (ESI+) calcd for $C_{23}H_{33}N_3NaO_4S$ 470.2084; found 470.2066 [M + Na].

(B) Preparation and characterization of gel materials

Characterization methods. Oscillatory rheological measurements were performed at 25 °C with an AR 2000 Advanced rheometer (TA Instruments) equipped with a Julabo C cooling system (Universität Regensburg). A 40 mm plain plate geometry (stainless steel) was used. Typically, the following experiments were carried out using 2 mL total gel volume: (a) dynamic strain sweep (DSS) was performed between 0.01% and 100% strain and a frequency of 1 Hz in order to estimate the strain value at which reasonable torque values were given; (b) dynamic frequency sweep (DFS) experiments were performed between 0.1 to 10 Hz and a strain of 0.1%; and (c) dynamic time sweep (DTS) measurements were performed with constant values of frequency and strain within the linear viscoelastic regime as determined with DSS and DFS (0.1% strain, 1 Hz frequency). Additionally, the thixotropic nature of the gels was confirmed with a three-step loop test: (1) application of a low shear strain (0.1%) at 0.1 Hz frequency for 10 min (*i.e.*, material is in gel state: $G' > G''$), (2) increase of the strain until the gel fractures (1000%) at 0.1 Hz frequency for 5 min (material turns into a viscous fluid: $G' < G''$), and (3) application of the initial strain value (0.1%) at 1 Hz frequency for 30 min (gel is recovered: $G' > G''$).

FTIR spectra were recorded using an Agilent Carry 630 spectrophotometer (Universität Regensburg) spectrophotometer.

Morphological characterization of the bulk samples was carried out by field emission scanning electron microscopy (FESEM), transmission electron microscopy (TEM) and atomic force microscopy (AFM). (a) FESEM: images were obtained with a Carl Zeiss Merlin field emission scanning electron microscope (0.8 nm resolution) equipped with a digital camera (SAI, Universidad de Zaragoza) and operating at 3 kV and 158 pA. Sample preparation: xerogel specimens were prepared by freeze-drying. Prior to imaging, a 5 nm sized Pt film was sputtered (40 mA, 30 seconds) on the samples placed on carbon tape. (b) TEM: images were recorded using a JEOL-2000 FXII transmission electron microscope (0.28 nm resolution) equipped with a CCD Gatan 694 digital camera (SAI, Universidad de Zaragoza) and operating at 200 kV (accelerating voltage). Sample preparation: 10 μL of the gel suspension was allowed to adsorb onto carbon-coated grids (300 mesh, from Aname). The grid was placed over a piece of filter paper in order to absorb the excess of solvent. (c) AFM: imaging was performed on a Multimode 8 (Bruker) instrument (LMA-INA, Zaragoza) in tapping mode at 0.5 Hz scanning rate using freshly cleaved mica surface as substrate and a single crystal silicon tip (TAP150A, 0.01–0.025 Ω cm, Antimony doped Si) at 128–152 kHz drive frequency. Drive amplitude ranged from 300 to 400 mV. Sample preparation: 10 μL of the alcogel suspension (ca. 5-fold dilution in MeOH) was placed on the substrate and homogeneously dispersed to form a thin layer that was allowed to dry in air overnight before measurement.

The growth of crystals in the gel phase was monitored using a Wild Makroskop M420 optical microscope equipped with a Canon Power shot A640 digital camera (Universität Regensburg). A polarization filter was used to observe the birefringence of the gels under polarized light.

Temperature-dependent ^{1}H-NMR studies were carried out on a 400 MHz Bruker Avance instrument (Universität Regensburg) equipped with a BVT 2000 heating system (Bruker BioSpin GmbH).

Powder X-ray diffraction (PXRD) patterns were collected on a STOE STADI P powder diffractometer (Universität Regensburg) (StartFragment Transmission mode, flat samples, Dectris MYTHEN 1k microstrip solid-state detector) with CuKα1 radiation operated at 40 kV and 40 mA. Conditions: (a) 0.015°, time 1200 s per step, 2 theta range 10–55° (short measurement); (b) StartFragment 0.015°, time 320 s per step, 2 theta range 2–90° (long measurement).

UV-vis spectra were recorded in a Varian Cary 50 Bio UV-visible spectrophotometer.

Critical gelation concentrations (CGC) were determined by adding solvent in several portions (0.1 mL each) into the vial until everything remained dissolved, precipitation and/or gelation took place upon heating–cooling (and/or ultrasound) treatment as described above. The initial concentration for gelation tests was 100 g L^{-1}.

Gel-to-sol transition temperatures (T_{gel}) were determined by the inverse-flow method by placing the sealed vials containing the organogels into a thermoblock (Fig. S1, ESI†), which was heated up at the rate of 2 °C min^{-1}. In this work, the temperature at which the gel started to break was defined as T_{gel}. The average values of at least two random experiments were given. These values were correlated with the first differential scanning calorimetry (DSC) endothermic transition of model using a DSC7 (Perkin Elmer) instrument (Universität Regensburg) at a scan rate of 2 °C min^{-1} under nitrogen atmosphere (gas flow rate = 20 mL min^{-1}). For the measurements, an appropriate amount of gel was placed into a pre-weighted Al pan (Perkin-Elmer), which was sealed and weight on a six-decimal plate balance. The pans were weighted again after each measurement to check for possible leakage.

General procedure for the preparation of organogels. Solvents (p.a. grade) used for gelation tests were purchased from commercial suppliers. In general, a certain amount of triturated squaramide was weighted and placed into a screw-cap vial (4.5 cm length × 1.2 cm diameter) and 1 mL of the corresponding solvent was added. Standard protocols for gel formation: (1) the heating–cooling protocol for the gel formation involved gently heating of the closed vial with a heat gun until the solid compound was completely dissolved, followed by spontaneous cooling of the isotropic solution to room temperature. (2) Alternatively, the heating–ultrasound protocol involved the application of ultrasound (ultrasound bath USC200TH, VWR™) directly after the heating. In each case, the material was classified as gel if no flow was observed upon turning the vial upside-down at room temperature. This phase was further confirmed by rheological measurements of model systems. Note: in some cases (see Table 1) the samples had to be pretreated in order to facilitate the dissolution of the compound during the standard protocols (i.e., heating–cooling or heating–ultrasound). The pretreatment consisted of gently heating followed by ca. 30 s sonication.

Phase-selective gelation experiments. Distilled water (1 mL) and 1-hexanol (1 mL) were added to compound **1** (7 mg, 0.014 mmol) placed into a screw-capped vial (4.5 cm length × 1.2 cm diameter). The vial was sealed and gently heated with a heat gun until the compound was completely dissolved. The mixture was sonicated for 1 min and kept undisturbed for 30 min, resulting in the gelation of the organic phase. The state of the material was established by turning the vial upside-down.

Responsiveness to external ions. Comparative experiments were made using the following metal salts: FeCl$_3$, Ni(OAc)$_2$·3H$_2$O, NiCl$_2$·6H$_2$O and CuCl$_2$. (A) Gels in methanol (1 mL) were prepared by heating–cooling using squaramide **1** at $c = 10$ g L^{-1}. After equilibration of the gels for 4 h, the desired metal salt solution (1 M in methanol) was added to each gel in 1 μL portions and left to rest for at least 18 h until the cation reached a concentration of 60 mM in the gel. The integrity of the gel phase was evaluated by visual inspection. (B) In order to crosscheck the values obtained in (A), 10 mg of compound **1** was added to 1 mL of the corresponding metal salt solution in methanol prepared at the critical concentration defined by experiment (A) (i.e., concentration where a response of the gel was evident to the naked eye). The mixture was heated for complete dissolution of the materials and subsequently cooled down to room temperature. The state of the bulk gel was monitored over time.

(C) Quantum mechanical calculations

All calculations were performed using the M06L functional,[63,64] which was combined with the 6-31+G(d,p) basis set[65]

Table 1 Gelation capacity of **1**, optical appearance of the gel phase, critical gelation concentration (CGC), gelation time, gel-to-sol transition temperature (T_{gel}), procedure for gel formation and temporal stability of the gels

Entry	Solvent[a]	Phase[b]	Optical appearance	CGC[e] (g L^{-1})	Gelation time[f]	T_{gel}[g] (°C)	Procedure[h]	Temporal stability[k]
1	Methanol	G	Transparent	7	24 ± 2 h	45	Heating–cooling	>6 months
2	2-Methylpentan-1-ol	G + U	nd	nd	nd	nd	Heating–cooling	nd
3	Butan-2-ol	G	Transparent	20	24 ± 6 h	nd	Heating–cooling[i]	>4 months
4	Ethanol	G	Translucent	5.8	10 min	46	**Heating–ultrasound**	Cryst. after 18 h
5	2-Methylpropan-2-ol	G	Translucent	3	5 min	57	**Heating–ultrasound**	>1 month
6	Butane-1,4-diol	G	Translucent	5.5	10 min	47	**Heating–ultrasound**[j]	>1 week
7	2-Methylpropan-1-ol	G	Translucent	4	1 min	67	**Heating–ultrasound**[j]	>1 week
8	Phenylmethanol	G	Opaque	21	8 min	42	**Heating–ultrasound**	>2 months
9	Acetone	G	Translucent	7.1	1 min	54	**Heating–ultrasound**[j]	>1 week
10	2-Methylbutan-2-ol	G	Translucent	3.3	5 min	70	**Heating–ultrasound**[j]	>2 weeks
11	Propan-1-ol	G + C	Opaque[d]	5.2	2 h	64	Heating–cooling	>6 months
12	Propan-1-ol	G	Translucent	5.2	5 min	56	**Heating–ultrasound**	>4 months
13	Pentane-1,5-diol	G	Opaque	10	15 min	47	Heating–cooling	>2 months
14	Pentane-1,5-diol	G	Translucent	6.1	12 min	36	**Heating–ultrasound**	>1 week
15	Butan-1-ol	G	Transparent	8.4	3.5 ± 0.25 h	39	Heating–cooling	>1 month
16	Butan-1-ol	G	Transparent	8.4	6 min	36	**Heating–ultrasound**	>1 month
17	Hexan-1-ol	G + C	Transparent	9.1	9 min	35	Heating–cooling[j]	>1 week
18	Hexan-1-ol	G	Transparent	7	1 min	75	**Heating–ultrasound**[j]	>2 months
19	3-Methylbutan-2-ol	G[c]	Transparent	5	20 ± 4 h	nd	Heating–cooling[j]	>1 month
20	3-Methylbutan-2-ol	G	Translucent	3.7	2 min	54	**Heating–ultrasound**[j]	>2 months
21	Pentan-2-ol	G	Transparent	5.5	11 ± 1 d	81	Heating–cooling	>1 month
22	Pentan-2-ol	G	Transparent	5.0	1 min	65	**Heating–ultrasound**	>2 months
23	2-Methylbutan-1-ol	G + C	Transparent	4.7	2.3 ± 0.15 h	65	Heating–cooling	Cryst. during gelation
24	2-Methylbutan-1-ol	G	Translucent	3.9	2 min	53	**Heating–ultrasound**	>1.5 months

[a] Solvent volume = 1 mL. Systematic IUPAC name is provided for each case. [b] Abbreviations: G = gel; U = undissolved gelator; C = crystals. [c] Approximately 10% of the total volume remained ungelled. [d] Cluster of white needles are visible within the fresh gel sample, which turned into a transparent gel after 12 days (*vide infra*). [e] Values calculated by the inverse-flow method. Estimated error ± 0.5–1 g L^{-1}. [f] Abbreviations: h = hour; min = minute; d = day. Unless otherwise noted, estimated error ± 1 min (for gelation times >1 min). [g] Estimated error ± 2 °C. [h] The heating–ultrasound treatment for the preparation of gels are highlighted in bold font. [i] To form this gel it was necessary to predissolve **1** in 20 μL of DMSO. [j] The sample was pretreated by heating–ultrasound as explain in the Experimental section. [k] The gels were stable at least for the indicated period. Symbol ">" indicates that the stability could possibly be much longer although it was not monitored. Abbreviation: nd = not determined due to unreliable variables; cryst = cyrstallization.

(*i.e.*, M06L/6-31+G(d,p) level) The M06L is a meta-hybrid generalized gradient approximation (GGA) functional with very good response under dispersion forces, improving one of the biggest deficiencies in density functional theory (DFT) methods. Thus, the M06L functional is able to describe the geometry and interaction energy of complexes stabilized by non-covalent interactions, including π–π stacking, with accuracy close to that of couple cluster calculations with both single and double substitutions.[66] All geometry optimizations were performed in methanol (ε = 32.6), which was described through a simple Self Consistent Reaction Field (SCRF) method. More specifically, the Polarizable Continuum Model[67,68] (PCM) was used in the framework of the M06L/6-31+G(d,p) level to represent bulk solvent effects.

Complexes formed by two interacting molecules (dimers) were considered for model squaramides **1**, **3**, **7**, **8** and **10**. For this purpose, around 50 starting geometries were constructed for each dimer by varying the relative position between the two interacting molecules. Accordingly, the formation of different specific and non-specific intermolecular interactions, as well as different geometries for each of such interactions,

were considered. All these starting arrangements were submitted to geometry optimization at the PCM-M06L/6-31+G(d,p) level. Interaction energies (ΔE_i) were corrected with the basis set superposition error (BSSE) by means of the standard counterpoise (CP) method.[69] Calculations were performed using the Gaussian 09[70] computer package.

Results and discussion

Design and synthesis of squaramides

In the frame of our interdisciplinary research program focused on the development of new hydrogen bond based functional molecules, some of us have recently focused on the synthesis of new squaramide structures,[60,71] due to their important ability for selectively binding through cooperative hydrogen bonds to different acceptors.[1,4–7] During the synthesis of squaramide **1** (Scheme 1) we observed a clear tendency to increase the viscosity of the solvent (*i.e.*, MeOH). Hence, we decided to investigate in detail the formation of supramolecular aggregates in solution,
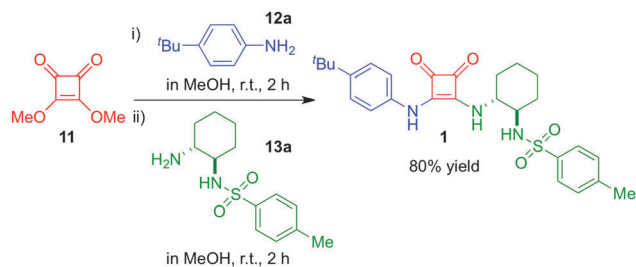
Scheme 1 One-pot synthesis of squaramide **1** in MeOH.

after taking also into consideration (a) the facile and scalable synthesis of this family of compounds, (b) the intrinsic potential as highly substituted scaffolds and (c) the isosteric relationship with ureas, which represent ubiquitous synthons in supramolecular chemistry[72] including the formation of softgels.[73]

In this context, unsymmetrical substituted squaramide **1** was easily accessible following our own developed procedure in a one-pot synthesis using equimolar amounts of commercially available 3,4-dimethoxycyclobut-3-ene-1,2-dione (**11**), 4-*tert*-butylaniline (**12a**) and *N*-((1*R*,2*R*)-2-aminocyclohexyl)-4-methyl-benzenesulfonamide (**13a**) in methanol at room temperature (Scheme 1). After 4 hours of reaction, squaramide **1** was obtained in very good yield (80%) after simple filtration as a powdered material with mesoscale ordering as indicated by PXRD analysis (Fig. S16, ESI†).

To correlate the structural functionalities of **1** with its gelation properties, we designed and synthesized the library of squaramides outlined in Fig. 1. Specifically, different analogous squaramides **7–10** were designed by incorporating substituents with different steric and electronic properties, following the same synthetic procedure.[60,71] For this purpose, squaramides **7** and **9**, with electron-withdrawing groups, or squaramide **8** with an electron-donating substituent in the aromatic ring, or **10** in the absence of the aromatic ring, were synthesized with the aim of modifying the basicity and/or conferring distinctive solvation properties to

these organic compounds, which is believed to play a key role on the gelation phenomena.[16–27] In all these cases (**1**, **7–10**), the stereochemical configuration and the structural core were maintained. Moreover, squaramides **2** and **3** were included for comparison with **1**, since we also observed that the viscosity of MeOH increased during their preparation. Additionally, and encouraged by our last work with urea-based compounds as efficient gelators,[74] we also carried out the preparation of squaramide **4**, which is the equivalent squaramide to the best urea compound used in our previous work.[74] Related with compound **4**, squaramide **5**, lacking the substituent in the aromatic ring, or **6**, bearing a methoxy group, were also explored.

All synthesized squaramides **1–10** were appropriately characterized after purification by a simple and straight filtration (see Experimental section).

Solubility and gelation properties

The gelation ability of compound **1** was initially screened for 34 different solvents using the heating–cooling protocol within a broad concentration range (Table 1 and Table S1, ESI†). For instance, squaramide **1** was found to be insoluble in dichloromethane, chloroform, ethyl acetate, diethyl ether, dibutyl ether, toluene, glycerol, 1,3-dichlorobenzene and water upon heating and/or sonication. Unexpectedly, **1** showed an unusual selectivity to form stable gels in a number of alcoholic solvents (alcogels), including primary, secondary, tertiary, lineal and branched alcohols. The only exception to this rule was the gel obtained in acetone. However, it should be considered that although acetone is present at >99% keto form at equilibrium, the formation of hydrogen bonding gel networks could stabilize to some extend the enol form of the acetone (2-propenol). In sharp contrast, no gelation tendency was detected for squaramides **2–10**. These results suggested the existence of unique molecular interactions and a hydrophilic/hydrophobic balance that favor the self-assembly of **1** in alcohols. This was later confirmed by computational studies (*vide infra*).

The gel nature of the samples was initially confirmed by the absence of flow upon turning the vial upside-down and further confirmed by oscillatory rheological measurements in model solvents (*vide infra*). The critical gelation concentration (CGC) values estimated for the gels obtained with **1** ranged between 3 and 21 g L^{-1} (see the Experimental section for the procedure). These values indicate that hundreds or thousands of solvent molecules are immobilized per gelator molecule (*e.g.*, the highest solvent/gelator ratio ~ 1750 : 1 was obtained in methanol). As far as we are aware, the only precedent in the literature describing the formation of an organogel with squaramides corresponds to a recent report from Ohsedo and co-workers[15] describing a series of squarylium monoalkylamides and dialkylamides. Therein, gelation was only observed in DMF (forming opaque gels) and in some cases only after cooling down the mixture to −15 °C.

Stable gels were classified in 3 different groups depending on the experimental protocol that was used for their preparation. The first group could only be formed by the classical heating–cooling protocol (entries 1–3), the second group could only be formed by applying heating and subsequent ultrasound treatment
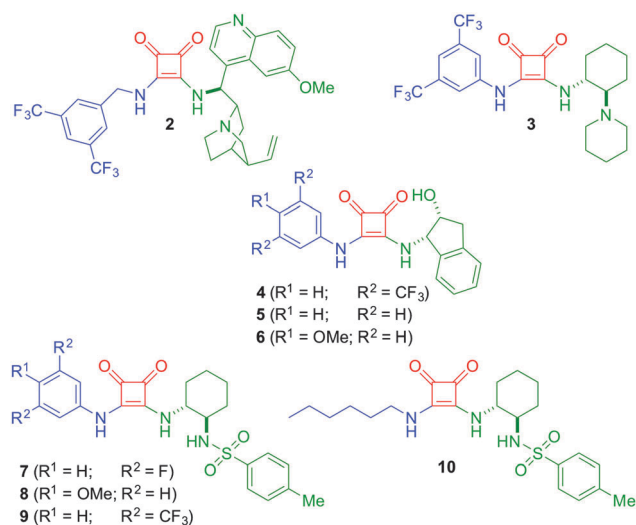

Fig. 1 Library of additional squaramides **2–10** synthesized for this work.

(entries 4–10) and the third group could be formed by any of these two methods (entries 11–24). Thus, *ca.* 47% of the obtained gels could be formed by heating–cooling, whereas *ca.* 82% could be prepared by a heating–ultrasound protocol (bold text). Although there is not an apparent correlation between the type of alcohol and the gel preparation method, heating followed by ultrasound was found to be a very convenient technique for the gelation of branched alcohols within minutes regardless the degree of substitution at the α-carbon. Based on these groups, we selected one model solvent of each group (*i.e.*, methanol, phenyl methanol and hexan-1-ol) for further characterization and comparisons. So obtained alcogels displayed different degree of translucency (Fig. 2). Such optical differences indicate the formation of aggregates of different sizes.

Ultrasound-induced gelation (sonogelation), mainly by solvent cavitation, has attracted much attention over the last few years.[75–78] During our work we found that the application of ultrasound after heating not only allowed the fabrication of stable gels that could otherwise (*i.e.*, *via* heating–cooling) not be formed, but also decreased the gelation time drastically (*e.g.*, entries 11, 15, 19, 21, 23 *vs.* entries 12, 16, 20, 22, 24, respectively). The most impressive case was pentan-2-ol that needed more than 10 days to be gelled by heating–cooling and only 1 min by heating–ultrasound even at lower concentration (entry 21 *vs.* entry 22). This is very appealing since the application of ultrasound to an already isotropic solution seems counterintuitive. However, sonication of the hot clear solution prior gelation may hinder the self-assembled system (non-entangled nanofibers) to fall into its lowest energy level making possible the formation of new gel networks. In addition, both the CGC was reduced in practically all cases in which the heating–ultrasound protocol was used instead of heating–cooling. This was also accompanied by certain reduction of the T_{gel} values. The case of hexan-1-ol should not be considered prematurely as an exception because

the heating–cooling protocol gave a combination of gel and crystals (entry 17 *vs.* entry 18). Remarkably, the dynamic nature of the gels was evidenced by a gradual increase over time of the T_{gel} for the gel prepared by heating–ultrasound reaching eventually the same value obtained by heating–cooling (*i.e.*, T_{gel} (fresh gel made in propan-1-ol) = 56 °C; T_{gel} (3-month old gel made in propan-1-ol) = 63 °C). As observed with the solid squaramide gelator **1**, the xerogels obtained by freeze-drying the corresponding alcogels were found to have mesoscale ordering as demonstrated by PXRD analysis (Fig. S16 and Table S2, ESI†). However, clear differences were observed between both spectra. The peaks observed for the solid sample (*i.e.*, as synthesized **1**) are centered at 2θ = 4.41°, 6.71°, 11.51°, 16.35° and 17.90°, corresponding to lattice spacings d of 20 Å, 13.16 Å, 7.68 Å, 5.42 Å and 4.95 Å, respectively (calculated from Bragg's law). In contrast, the peaks centered at 11.51° and 17.90° disappeared completely in the xerogel sample, whereas all other peaks slightly shifted to low angles (*i.e.*, 3.96°, 6.18° and 15.70°, respectively); these peaks correspond to d values of 22.28 Å, 14.3 Å and 5.64 Å, respectively. This suggests that the interactions of the solvent molecules with the gelator (or gelator-based aggregates) during gelation cause disorder and expansion of the potential crystal packing of the gelator, at least to some extent.

In addition, UV-vis analysis during the sol-to-gel transition did not show a shift of the absorption maximum (Fig. S17, ESI†), suggesting that the aggregation mode of **1** in solution (and probably in the solid state, *vide infra*) resembles that in the gel phase.

Phase-selective gelation capacity. Very interestingly, squaramide **1** was also able to gel selectively the organic phase of alcohol/water mixtures. In principle, such phase-selective gelation is always challenging due to the expected alteration of the hydrogen bonding network.[79] As a proof-of-concept, **1** (c = 7 g L^{-1}) was dissolved in 1 : 1 v/v water/hexan-1-ol by heating and subsequently submitted to sonication for 1 min. After 30 min of resting, only the organic phase was completely gelled, which was stiff enough to hold the liquid water phase upon inversion of the vial. Due to the partial solubility of hexan-1-ol in water (*i.e.*, 5.9 g L^{-1} at 20 °C), the aqueous phase was not completely clear after gelation of the alcohol. However, after 24 h the water phase got clearer and the organic phase more turbid (Fig. 3). This was presumably due to the disruption of the microemulsion and diffusion of the tiny fraction of gelator molecules that could be trapped into the aqueous phase. Phase-selective gelation using water-soluble alcohols such as methanol was not successful. The addition of 10–20% water either before or after gel formation resulted in the collapse of the gel after several days caused by a thick precipitation (Fig. S14, ESI†).

Thermal and temporal stability of alcogels

In general, the supramolecular gels were thermoreversible and stable to multiple heating–cooling cycles. The gel-to-sol transition temperatures (T_{gel}) were estimated by the inverse flow method (IFM). Due to the dependence of this method with the cooling rate and thermal history of the sample, we confirmed the good agreement of the T_{gel} with the first endothermic transition
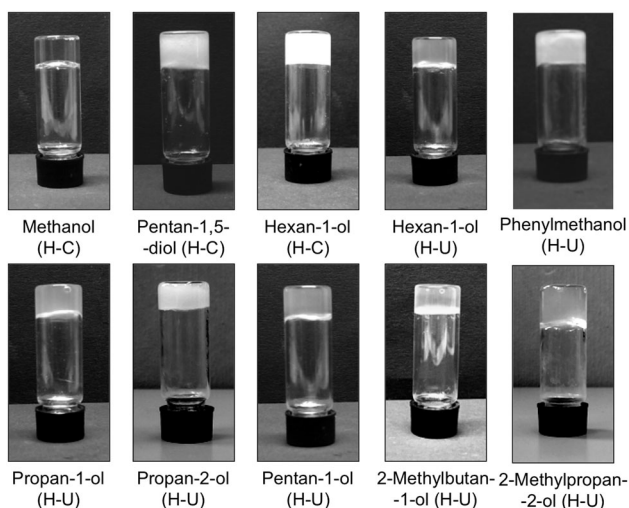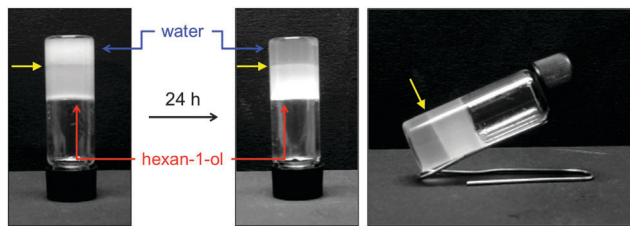

Fig. 2 Representative photographs of upside-down vials containing organogels made of gelator **1** in different alcohols prepared at the corresponding CGC (Table 1) *via* heating–cooling (H-C) or heating–ultrasound (H-U).

Fig. 3 Phase-selective gelation and change in opacity of hexan-1-ol/water mixture after 24 h (gelator **1**, c = 7 g L^{-1}). Total volume = 2 mL. Yellow arrow indicates the boundary between phases.

observed by differential scanning calorimetry (DSC) of a model gel (Fig. S5, ESI†).

As usually observed in physical gels, T_{gel} values increased as the gelator concentration increased until reaching a plateau before visible crystal nucleation. For example, T_{gel} of the gel made in methanol increased *ca.* 23 °C upon increasing *ca.* 3-fold the concentration of **1** with respect to the CGC (7 g L^{-1}). Crystal formation was observed over 22 g L^{-1} within 10 min (Fig. 4). Although these results might be in agreement with the formation of more entangled networks at higher gelator concentrations, the change in T_{gel} is likely due to solution thermodynamics where the phase boundary, or liquidus line, increases at low concentration and levels off at higher concentration.

Very interestingly, in several cases we have observed an enhancement of both the gelation kinetics and the gel stability when the gels were reformed after being thermally destroyed for the first time. We believe that the gel-to-sol thermal transition could be controlled to avoid the complete dissociation of the supramolecular network (even when behaving as a fluid from the rheological standpoint). This could preserve the thermodynamically more stable aggregates through a self-sorting mechanism, thus providing a more robust starting platform for rebuilding the gel structure. We believe that such "preformation hypothesis" could be more general and become an important contribution to the gelation theory. We are currently studying this in detail and we will publish our results at due course.
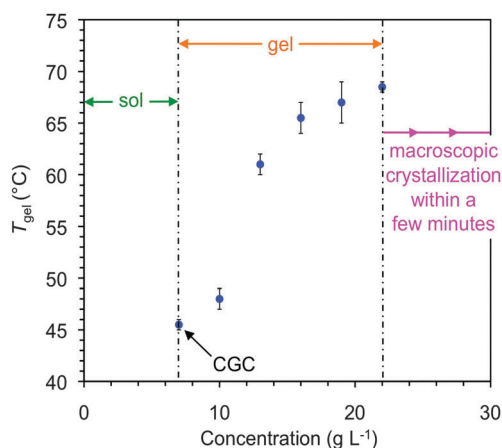
On the other hand, gel-to-crystal transitions have been previously related to Ostwald rule of stages.[80,81] The subtle equilibrium between the metastable gel phase and the thermodynamically stable crystalline phase[82–85] could also be monitored in several of our alcogels. For instance, macroscopic crystallization in the form of long needles was observed first at the interface between air and the developing gel phase made of **1** in 2-methyl-butan-1-ol, hexan-1-ol or propan-1-ol *via* heating–cooling (Fig. 5). Nevertheless, the robustness of the gel phase allowed in most of the cases the coexistence of crystalline and gel phases for at least one month supporting the inversion of the test tube. In general, the alcogels prepared *via* heating–ultrasound remained stable for several months without visible crystallization when stored in dark at room temperature.

Although gel-to-gel transitions have already been reported,[86–89] it is still a rare phenomenon. The gels made in phenylmethanol showed an optical transition from transparent to opaque within 30 min at the CGC (Fig. 6A). This behavior is typically observed during the growth of fibrilar aggregates over time. Intriguingly, the uncommon opposite phenomenon was observed with the alcogel prepared in propan-1-ol by heating–cooling. In this case, initial macroscopic crystallization was observed during the gelation process leading to a transient opaque gel, which turned into a thermodynamically stable transparent gel within 12 days (Fig. 6B). However, additional detailed experimentation to determine the exact packing arrangement of the gelator molecules, and prove its gradual change, is still necessary in order to confirm the apparent gel-to-gel transition in this case.

Influence of gelator enantiopurity on gel formation

Chirality plays a fundamental role in the formation of supramolecular gel networks.[90] Therefore, we also examined the influence of the enantiomeric purity of **1** on its gelation ability. Samples with different enantiomeric excesses (ee) were prepared by combining (*R*,*R*)-**1** with the appropriate amount of the racemic compound, which was prepared following the general synthetic procedure using the corresponding racemic diamine (see Experimental section). Stable-to-inversion gels could only be formed with the enantiomerically pure (*R*,*R*)-**1**. The squaramide with 80% ee yielded a weak partial gel after 88 h. Macroscopic crystallization
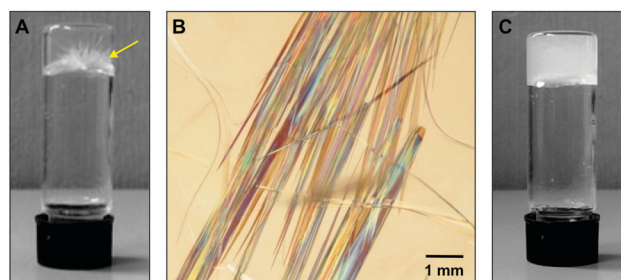

Fig. 4 Phase diagram and variation of T_{gel} as a function of the concentration of gelator **1** in methanol.

Fig. 5 (A) Digital photograph showing crystal growth in the gel made of **1** in 2-methylbutan-1-ol (c = 4.7 g L^{-1}) by heating−cooling. (B) Optical microscope picture of the crystals observed in (A). (C) Gradual crystal growth observed during the gelation of hexan-1-ol using **1** (c = 9.1 g L^{-1}) and the heating−cooling protocol. The gelator concentration corresponds to the CGC (Table 1).
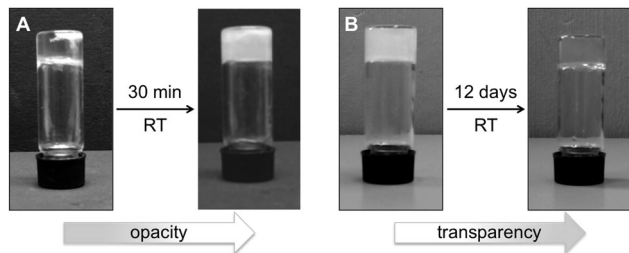
Fig. 6 (A) Transparent-to-opaque transition recorded for the gel made of **1** in phenylmethanol (c = 21 g L^{-1}) within 30 min after gel formation *via* heating–ultrasound. (B) Opaque-to-transparent transition observed in the gel made of **1** in propan-1-ol (c = 5.2 g L^{-1}) within 12 days after gel formation *via* heating–cooling. The concentrations of gelator correspond to the CGC (Table 1).

of the gelator was observed after 9 days. The use of **1** with ee < 80% led to snow flake-like precipitation of **1** without any gel formation (Fig. 7).

Driving forces for molecular aggregation

The comparison of FTIR spectrum of solid squaramide **1** with those of the xerogel (prepared by freeze-drying the corresponding alcogel) and **1** in solution revealed only slight alteration with small frequency shifts to lower wavelengths ($\Delta\lambda < 4$ cm^{-1}) for characteristic peaks (*e.g.*, stretching absorptions bands for C=O $\sim$1658–1794 cm^{-1}; secondary amines $\sim$3210–3345 cm^{-1}; aromatic C–H $\sim$2910–3005 cm^{-1}; aromatic C–N $\sim$1265–1370 cm^{-1}) (Fig. S4, ESI†). This suggests that **1** may also be aggregated in the solid state involving intuitive hydrogen bonding and π-stacking interactions similarly to its analogue urea-based organogelator.[74] This is also in agreement with the results obtained by UV-vis measurements during the sol-to-gel transition (*vide supra*).

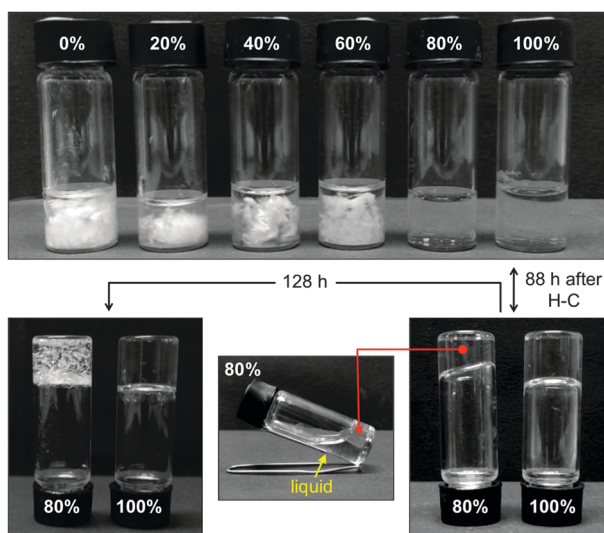On the other hand, temperature-dependent ^{1}H-NMR experiments could provide additional information regarding

Fig. 7 Influence of enantiomeric purity of gelator **1** on its gelation ability in methanol (c = 7 g L^{-1}) monitored over time. Enantiomeric excesses are given in percentages.

phase interconversions. However, it should be noted that NMR signals of gelator molecules are unlikely to be observed in the gel phase due to long correlation times. Therefore, the observed signals are typically ascribed to small amounts of gelator molecules dissolved in the immobilized solvent.[91,92] Preliminary NMR measurements of the alcogel made of **1** in d_4-methanol with increasing temperature from 25 °C to 60 °C showed gradual chemical shifts (δ) of almost all protons of **1** suggesting at least conformational changes and/or expected modification in the aggregation pattern (*e.g.*, through hydrogen bonding, π-stacking and/or electrostatic interactions) (Fig. S6, ESI†).

In contrast to the PXRD pattern of compound **1**, non-gelators **2–10** showed additional peaks after 17° (Fig. S16 and Table S2, ESI†). Some of these compounds showed even higher crystallinity than the squaramide gelator **1** (*e.g.*, compounds **5**, **7**). On the other hand, the two major peaks at low angle (around 4° and 6°) found in the xerogel of **1** do not appear in the other solid compounds, except compound **7** that also showed two peaks in the same region as well as the new additional peaks at higher angle. In other compounds (*e.g.*, compounds **6**, **8**) only one of the two mentioned peaks was present together with the additional peaks at higher angle. Thus, although we can not provide a unique reason why squaramide **1** is the only one that forms gels, it seems that the complex gelation phenomenon, frequently defined as a "frustrated crystallization", finds here a unique example, where both the structure of the gelator and the solvent must play a crucial and synergistic role in turning the phase balance towards gelation in the case of compound **1** *vs.* **2–10**.

In order to gain a clearer insight into the potential aggregation mode of **1** and its unique gelation ability, comparative PCM-M06L/6-31+G(d,p) calculations in methanol were carried out on model dimers of **1**, **3**, **7**, **8** and **10**. It should be remarked that this methodology, which is not appropriated to evaluate why only alcohols and acetone give gels, is suitable to describe precisely specific interactions and evaluate differences among the inter-action patterns in the different dimers. Moreover, **1**, **3**, **7**, **8** and **10** are similar enough to represent the solvent using a polarized continuum dielectric medium, like the PCM one. Accordingly, these calculations do not intend to ascertain the role of the solvent in the gelation mechanism but differences among molecules in a given solvent. For simplicity, analyses of the results were restricted to the minima of lower relative energy, which correspond to those with more attractive interaction energies (ΔE_i). Thus, 13 of the 22 minima obtained for **1** exhibit ΔE_i values lower than -6 kcal mol^{-1}. More specifically, ΔE_i ranges from -26.1 to -6.1 kcal mol^{-1} (Fig. 8).

Inspection of the lowest energy dimer (Fig. 9A) revealed that the squaramide moiety of each molecule is involved in different intermolecular interactions. In addition to the conventional N–H···O hydrogen bond, which involves the squaramides of the two molecules, this dimer also exhibits stabilizing N–H···π and C–H···π intermolecular interactions. In addition to such interactions, the two molecules involved in this complex show intramolecular π···π stacking interactions, as is illustrated for one of the two monomers (Fig. 9A, right). These attractive interactions involve three aromatic rings forming a multiple
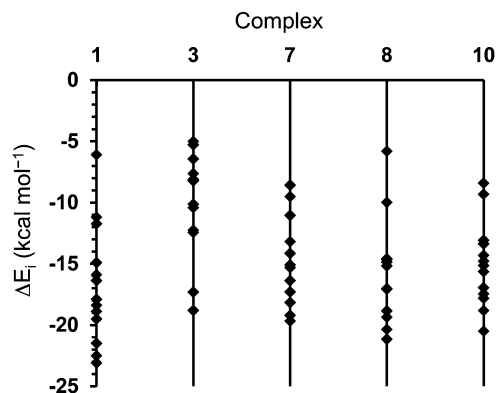
Fig. 8 For the most stable complexes of each family, representation of the interaction energy (ΔE_i) of complexes calculated for **1**, **3**, **7**, **8** and **10** with $\Delta E_i \leq 5.0$ kcal mol^{-1}.

phenyl···phenyl and squaramide···phenyl stacking, which provide extra stability to the complex. Moreover, careful inspection of the complexes $\Delta E_i < -15$ kcal mol^{-1} (9 of the 13 minima represented in Fig. 8) revealed that similar inter- and intramolecular interactions coexist in all cases. However, although in all cases intramolecular interactions involve the stacking of the three aromatic rings, intermolecular interactions typically consists of two C═O···H–N hydrogen bonds involving the squaramides or a single S═O···H–N hydrogen bond. This is illustrated in Fig. 9B and C, which display the second ($\Delta E_i = -22.5$ kcal mol^{-1}) and third minima ($\Delta E_i = -21.5$ kcal mol^{-1}) in the energy ranking, respectively.

Complexes of **3** tend to be stabilized by intermolecular N–H···O hydrogen bonds and N–H···π interactions, while intramolecular interactions consists of N–H···N hydrogen bonds (Fig. 10). It should be noted that, in comparison with **1**, the lack of the third aromatic ring absence precludes the formation of intramolecular π···π stacking interactions. Comparison of complexes obtained for **1** and **3** suggests that both the lower number of intermolecular hydrogen bonds and the lack of intramolecular π···π stacking interactions are responsible for the relatively high ΔE_i values and poor stability of the latter with respect to the former.

In comparison with **3**, the interaction patterns of complexes derived from **7**, **8** and **10** are more similar to those observed for **1**, even though there are also some differences among the formers and the latter. Thus, the lower energy complexes calculated for **7** and **10** exhibited two N–H···O intermolecular hydrogen bonds (Fig. S19 and S20, ESI,† respectively), while those derived from **8** show only one of such interactions (Fig. S21, ESI†). Furthermore, no N–H···π and C–H···π intermolecular interactions were detected in **7**, **8** and **10**. Accordingly, intermolecular interactions seem to be weaker for **8** than for **7**, **10** and, specially, **1**.

Regarding to intramolecular interactions **7**, **8** and **10** display π···π stacking, even though they also present some relevant differences. Specifically, such π···π interactions are apparently weaker for **7** and **10** than those obtained for **1** and **8**. Thus, three aromatic rings participate in each π···π interaction identified in complexes of the two latter compounds (Fig. 9 and Fig. S21, ESI†),
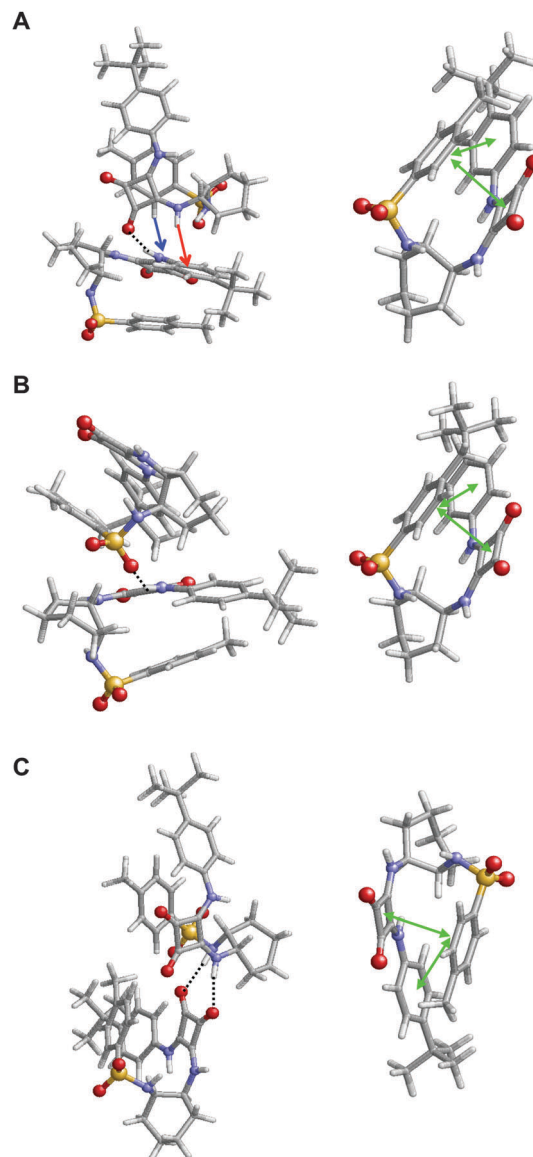

Fig. 9 Representation of the three most stable complexes obtained for **1**: (A) $\Delta E_i = -26.1$ kcal mol^{-1}; (B) $\Delta E_i = -22.5$ kcal mol^{-1} and (C) $\Delta E_i = -21.5$ kcal mol^{-1}. Intermolecular (left) and intramolecular (right) interactions are displayed for the complex and a single molecule of the complex, respectively. Hydrogen bonds are represented by black dashed lines, N–H···π and C–H···π interactions by read and blue arrows, respectively, and intramolecular π···π stacking interactions by green double arrows.

while only two aromatic rings are involved in those found in the complexes of the formers (Fig. S19 and S20, ESI†). The reduction in the intensity of π···π interactions for **7** and **10** has been attributed to the repulsive effects provoked by the fluoride substituents and to replacement of an aromatic ring by an aliphatic chain, respectively. These results clearly indicate that dimers calculated for **1** show a large and complex network of inter- and intramolecular interactions that provides an additional stability to the complex. This network of interactions becomes weaker and smaller for the complexes that involve the rest of compounds and, therefore, such extra stability disappears.
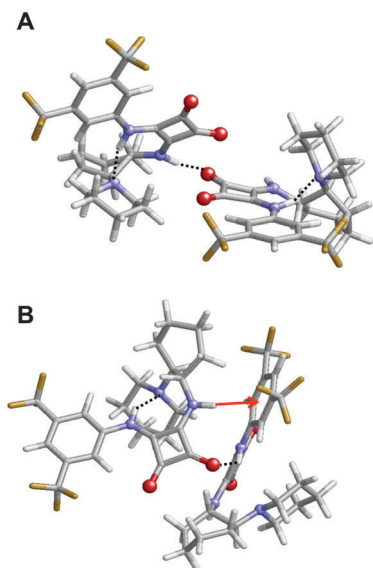
Fig. 10 Representation of the two most stable complexes obtained for **3**: (A) ΔE_i = −18.8 kcal mol^{-1} and (B) ΔE_i = −17.3 kcal mol^{-1}. Intermolecular and intramolecular interactions are displayed for each complex. Inter- and intramolecular hydrogen bonds are represented by black dashed lines, and N−H⋯π interactions by read arrows.

Additional PCM-M06L/6-31+G(d,p) calculations were performed for dimers of **1** in water and chloroform (ε = 4.7 and 78.4, respectively). Results were similar to those obtained in methanol suggesting that the influence of the solvent on the gelation ability of this compound is not due to simple electrostatic effects induced by the polarization of the solvent but to the role of the first solvation shell in the network of inter- and intramolecular interactions discussed above. Unfortunately, continuum models, like PCM, are unable to describe the effects associated to solute⋯solvent interactions in the first solvation shell. Therefore, considering the remarkable selectivity of the gelator for alcoholic solvents, the differences in PXRD patterns (*e.g.*, as synthesized gelator *vs.* xerogel) and the standard gelation mechanism associated to supramolecular gels,[1,43–50] we should not dismiss the potential role of at least some solvent molecules acting, for instance, as bridges between gelator molecules. This has been proved by additional PCM-M06L/6-31+G(d,p) calculations on complexes formed by two interacting molecules of **1** and two methanol molecules positioned between them (Fig. S22, ESI†). It is worth noting that each molecule of **1** interacts simultaneously with methanol and with the second molecule of **1**. Unfortunately, the theoretical methodology used in this work is suitable to examine the ability of the different compounds to form intermolecular interactions but it is not appropriated for a systematic exploration of this bridge-like gelation mechanism. Thus, due to the huge number of possibilities, other theoretical approaches based on statistical sampling procedures would be more appropriated for such purpose.

Morphological properties of alcogels

Field emission scanning electron microscopy (FESEM) of the corresponding xerogels showed a remarkable influence of the solvent on the morphologies. For instance, straight laths of *ca.* 0.2–1.4 μm in width were observed for gel made in phenylmethanol (Fig. 11B), whereas dense fibrilar networks with entangled fibers of *ca.* 10–20 nm in diameter were characteristic of the gels made in hexan-1-ol (Fig. 11C and D) and methanol (Fig. 11A). The exact molecular mechanism associated with each morphology remains unclear. No major differences were apparently observed for the gel phase obtained either by heating–cooling or heating–ultrasound for the gel made in hexan-1-ol (Fig. 11C, D and Fig. S8, ESI†). However, transmission electron microscopy (TEM) seems to reveal a less dense fibrilar network for the gel prepared by heating–ultrasound (Fig. 12 and Fig. S9, ESI†).

As expected, complementary fibril structures with average heights between *ca.* 4 nm and 10 nm were also observed by atomic force microscopy (AFM) (Fig. 13). Certain fiber helicity was detected by FESEM and AFM imaging (Fig. S10, ESI†). Although we have recorded images of the nanostructures by different techniques in order to identify any possible artifact, it should be emphasized that important changes in the structures could occur during preparation of the samples and, therefore, the interpretation of the images should always be done carefully without overselling.

In addition, the anisotropic and thermoreversible features of the alcogels allowed turning on/off their birefringence under polarized light (Fig. S11, ESI†). The ability to control the refractive index of soft materials constitutes an important property for applications in optical devices.[93]

Rheological properties of alcogels

The viscoelastic properties of the model gels were confirmed by oscillatory rheological measurements (Fig. S7, ESI†). The storage (G') and loss modulus (G'') were measured at room temperature as a function of the shear strain (dynamic strain
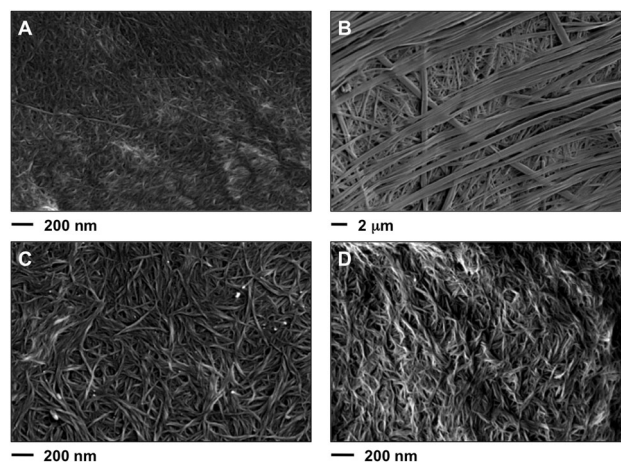

Fig. 11 Representative FESEM images of the xerogels prepared by freeze-drying of the corresponding organogels made of **1** in different solvents at their CGC (Table 1). (A) Methanol (heating−cooling, c = 7 g L^{-1}), (B) phenylmethanol (heating−ultrasound, c = 21 g L^{-1}), (C) hexan-1-ol (heating−ultrasound, c = 7 g L^{-1}) and (D) hexan-1-ol (heating−cooling, c = 9.1 g L^{-1}). Note: the selected images are representative of the bulk material. For additional images see ESI.†
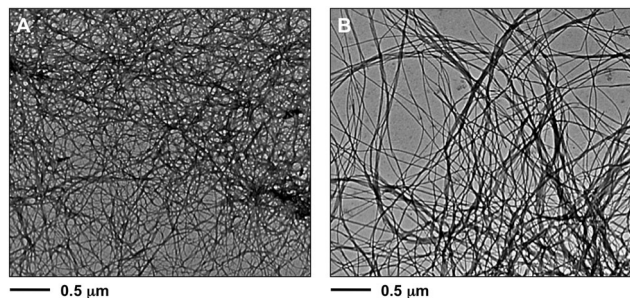
Fig. 12 Representative TEM images of xerogels of the corresponding organogels made of **1** in different solvents at the CGC (Table 1): (A) methanol (heating–cooling, $c = 7$ g L^{-1}), (B) hexan-1-ol (heating–ultrasound, $c = 7$ g L^{-1}). Note: the selected images are representative of the bulk material. For additional images see ESI.†

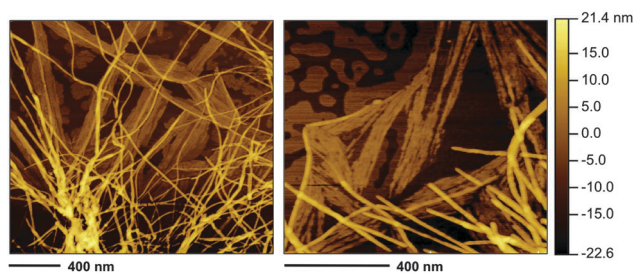Fig. 13 Representative AFM images of the gel made of **1** in methanol (heating–cooling) at the CGC ($c = 7$ g L^{-1}). Note: the selected images are representative of the bulk material. For additional images see ESI.†

sweep, DSS) and the frequency (dynamic frequency sweep, DFS) to define the linear viscoelastic regime of the material (Fig. 14 and Fig. S7, ESI†). Although all gels should be defined as weak gels according to the moduli values, reasonably constant values of the tan δ (G''/G') during the measurements indicated a relative good tolerance of the materials towards low external forces. Moreover, the value of the storage modulus was always *ca.* one order of magnitude higher than the loss modulus. The aging stability of the gels at room temperature was confirmed by dynamic time sweep (DTS) measurements within the pre-determined linear limits (*i.e.*, 0.1% strain, 1 Hz frequency).

Furthermore, these gels were also found to be thixotropic,[94] a key property for real-life applications of many gel-based materials.[95] This behavior was confirmed by a three-steep rheological loop test consisting of (1) application of shear strain as defined by DTS experiments ($G' > G''$), (2) subsequent increase of the strain until the gel collapses ($G' < G''$) and (3) return to the starting strain value ($G' > G''$). Full recovery of the gel strength was observed within seconds after each cycle (Fig. 15). This self-healing behavior was also macroscopically observed upon vigorous shaking of the vial containing the bulk gel followed by a resting period (Fig. S18F, ESI†).

Responsiveness to external ions

Since squaramide derivatives are known to coordinate to anions at the N–H groups and to cations at the carbonyl moiety, we expected a response of the alcogels to the presence of
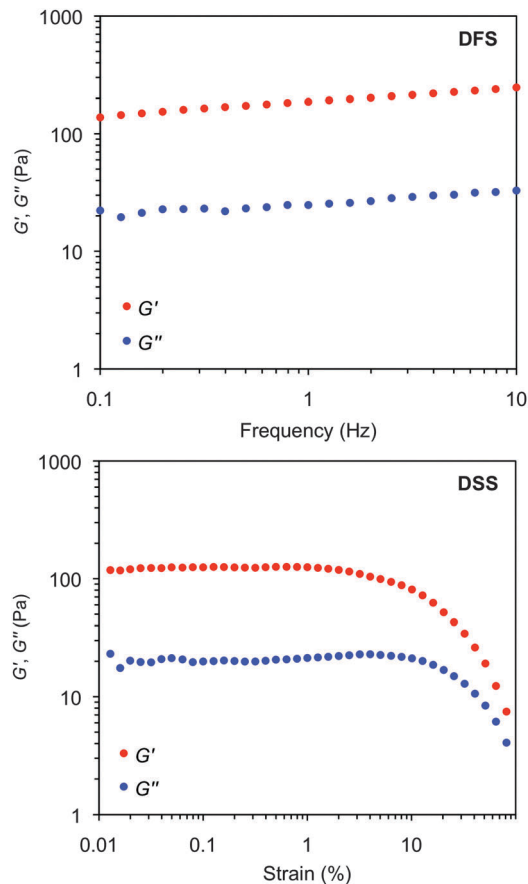

Fig. 14 Representative oscillatory rheological plots of the model gel made of **1** in methanol at CGC ($c = 7$ g L^{-1}). Top: DFS experiment. Bottom: DSS experiment.

external ions. In order to confirm this, a small amount of different metal salt solutions in methanol (*i.e.*, FeCl$_3$, Ni(OAc)$_2$·3H$_2$O, NiCl$_2$·6H$_2$O, Cu(NO$_3$)$_2$ and CuCl$_2$) were layered over 1 mL of the model gel made of **1** in methanol ($c = 10$ g L^{-1}). Potential complexation of the ions with the gelator molecule may disrupt

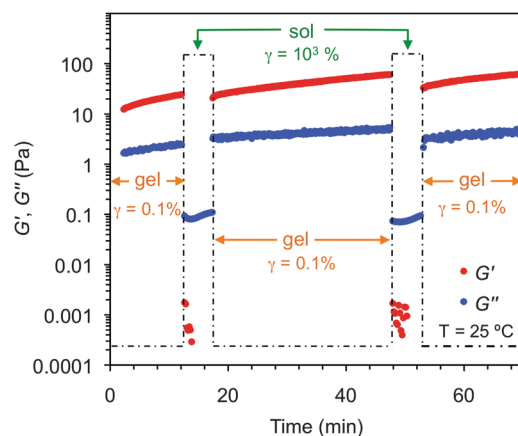Fig. 15 Rheological loop test of the gel made of **1** in butan-1-ol at CGC ($c = 8.4$ g L^{-1}). Steps: (1) 1 Hz, 0.1% strain, 10 min; (2) 0.1 Hz, 1000% strain, 5 min; (3) 1 Hz, 0.1% strain, 30 min. Steps 2 and 3 were repeated for a second cycle.
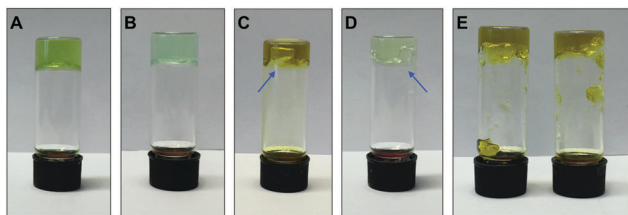
Fig. 16 Effect of external ions on the stability of the gel made of **1** in methanol ($c = 10$ g L^{-1}). (A) 60 mM $CuCl_2$: stable gel. (B) 60 mM $Ni(OAc)_2 \cdot 3H_2O$: stable gel. (C) 30 mM $FeCl_3$: gel decomposition in 3.5 h. (D) 60 mM $NiCl_2 \cdot 6H_2O$: gel decomposition within 6 h. (E) Left: Addition of **1** to metal solution (30 mM $FeCl_3$) followed by heating–cooling. Right: Addition of metal solution (30 mM $FeCl_3$) to preformed gel *via* heating–cooling. Gel colours correspond to the colours of the metal salt solutions.

the nanofibers causing the gradual collapse of the gel network. As a matter of fact, this was observed in preliminary experiments upon addition of either 30 mM $FeCl_3$ or 60 mM $NiCl_2 \cdot 6H_2O$ stock solutions within 3.5 h and 6 h, respectively (Fig. 16C and D). Interestingly, the addition of 60 mM $CuCl_2$ or $Ni(OAc)_2 \cdot 3H_2O$ did not cause visible decomposition of the gel network within 72 h (Fig. 16A and B), suggesting different effects of metal ions and counterions on the gel stability. The response of the gel was independent on the procedure used for the preparation of the hybrid material (Fig. 16E). Future research is still necessary to elucidate the exact nature of the metal complexes and the dominant mechanism for the gel destruction.

Conclusions

The foregoing results demonstrate that chiral *N*,*N*′-disubstituted squaramide **1** self-assembles selectively in a large variety of alcohols at concentrations ranging from 3 to 21 g L^{-1}. This phenomenon leads to the formation of nanostructured supramolecular alcogels with the ability to response to thermal, mechanical, optical and chemical stimuli. Experimental gelation tests and computer modeling of a series of structurally related squaramides (**2–10**) demonstrated the existence of a unique combination of non-covalent molecular interactions and favorable hydrophobic/hydrophilic balance in **1** that drive the growth of stable gel networks. The application of a heating ultrasound protocol instead of the classical heating–cooling cycle allows not only the formation of alcogels that could otherwise not be formed, but it also decreases both CGC and gelation times in comparison to the heating–cooling treatment. Moreover, the nature of the solvent has a remarkable effect on the morphology of the aggregates (*e.g.*, straight laths, entangled fibers) and some gels also exemplify the strong competition between gelation and macroscopic crystallization typically observed in weak physical gels. Thixotropic behavior and phase selective gelation of non-miscible alcohol/water mixtures are other interesting features of these alcogels.

This work opens new possibilities for the use of squaramides in materials synthesis beyond their classical applications in catalysis, sensors and medicine. However, additional examples of other squaramide-based gelators with broader gelation abilities

and higher mechanical stabilities are still necessary in order to establish the real potential of this building block for the preparation of supramolecular gels. Investigations related to the described "preformation hypothesis" within the overall gelation theory for similar systems, as well as the study of the apparent gel-to-gel transitions are currently underway in our laboratories and the results will be published at due course.

Acknowledgements

Notes and references

1 R. I. Storer, C. Aciro and L. H. Jones, *Chem. Soc. Rev.*, 2011, **40**, 2330.

2 J. P. Malerich, K. Hagihara and V. H. Rawal, *J. Am. Chem. Soc.*, 2008, **130**, 14416.

3 J. R. Merritt, L. L. Rokosz, H. N. Kingsley, B. Kaiser, W. Wang, T. M. Stauffer, L. E. Ozgur, A. Schilling, G. Li, J. J. Baldwin, A. G. Taveras, M. P. Dwyer and J. P. Chao, *Bioorg. Med. Chem. Lett.*, 2006, **16**, 4107.

4 J. Alemán, A. Parra, H. Jiang and K. A. Jørgensen, *Chem. – Eur. J.*, 2011, **17**, 6890.

5 J. V. Alegre-Requena, *Synlett*, 2014, 298.

6 P. Chauhan, S. Mahajan, U. Kaya, D. Hack and D. Enders, *Adv. Synth. Catal.*, 2015, **357**, 253.

7 F. R. Wurm and H.-A. Klok, *Chem. Soc. Rev.*, 2013, **42**, 8220.

8 R. Prohens, A. Portell, C. Puigjaner, S. Tomàs, K. Fujii, K. D. M. Harris, X. Alcobé, M. Font-Bardia and R. Barbas, *Cryst. Growth Des.*, 2011, **11**, 3725.

9 R. Prohens, A. Portell and X. Alcobé, *CrystEngComm*, 2012, **12**, 4548.

10 R. Prohens, A. Portell, C. Puigjaner, R. Barbas, X. Alcobé, M. Font-Bardia and S. Tomàs, *CrystEngComm*, 2012, **14**, 5745.

11 A. Portell, M. Font-Bardia and R. Prohens, *Cryst. Growth Des.*, 2013, **13**, 4200.

12 A. Portell and R. Prohens, *Cryst. Growth Des.*, 2014, **14**, 397.

13 B. Soberats, L. Martinez, E. Sanna, A. Sampedro, C. Rotger and A. Costa, *Chem. – Eur. J.*, 2012, **18**, 7533.

14 C. López, E. Sanna, L. Carreras, M. Vega, C. Rotger and A. Costa, *Chem. – Asian J.*, 2013, **8**, 84.

15 Y. Ohsedo, M. Miyamoto, A. Tanaka and H. Watanabe, *New J. Chem.*, 2013, **37**, 2874.

16 D. J. Abdallah and R. G. Weiss, *Adv. Mater.*, 2000, **12**, 1237.

17 P. Terech and R. G. Weiss, *Chem. Rev.*, 1997, **97**, 3133.

18 J. H. van Esch and B. L. Feringa, *Angew. Chem., Int. Ed.*, 2000, **39**, 2263.

19 O. Gronwald and S. Shinkai, *Chem. – Eur. J.*, 2001, **7**, 4328.

20 K. Hanabusa, *Springer Ser. Mater. Sci.*, 2004, **78**, 118.

21 *Molecular Gels: Materials with Self-Assembled Fibrillar Networks*, ed. R. G. Weiss and P. Terech, Springer, Dordrecht, 2006.

22 M. George and R. G. Weiss, *Acc. Chem. Res.*, 2006, **39**, 489.

23 X. Y. Liu, *Top. Curr. Chem.*, 2005, **256**, 1.

24 M. de Loos, B. L. Feringa and J. H. van Esch, *Eur. J. Org. Chem.*, 2005, 3615.

25 G. C. Maity, *J. Phys. Sci.*, 2007, **11**, 156.

26 E. Zaccarelli, *J. Phys.: Condens. Matter*, 2007, **19**, 323101.

27 S. Banerjee, R. K. Das and U. Maitra, *J. Mater. Chem.*, 2009, **19**, 6649.

28 A. Vintiloui and J.-C. Leroux, *J. Controlled Release*, 2008, **125**, 179.

29 J. H. Jung and S. Shinkai, *Top. Curr. Chem.*, 2004, **248**, 223.

30 N. M. Sangeetha and U. Maitra, *Chem. Soc. Rev.*, 2005, **34**, 821.

31 R. V. Ulijn and A. M. Smith, *Chem. Soc. Rev.*, 2008, **37**, 664.

32 M. O. M. Piepenbrock, G. O. Lloyd, N. Clarke and J. W. Steed, *Chem. Rev.*, 2010, **110**, 1960.

33 S. Li, V. T. John, G. C. Irvin, S. H. Bachakonda, G. L. McPherson and C. J. O'Connor, *J. Appl. Phys.*, 1999, **85**, 5965.

34 T. Kato, *Science*, 2002, **295**, 2414.

35 J. Puigmarti-Luis, V. Laukhin, A. P. del Pino, J. Vidal-Gancedo, C. Rovira, E. Laukhina and D. B. Amabilino, *Angew. Chem., Int. Ed.*, 2007, **46**, 238.

36 W. Kubo, S. Kambe, S. Nakade, T. Kitamura, K. Hanabusa, Y. Wada and S. Yanagida, *J. Phys. Chem. B*, 2003, **107**, 4374.

37 C. Sanchez and M. Llusar, *Chem. Mater.*, 2008, **20**, 782.

38 A. Friggeri, K. J. C. van Bommel and S. Shinkai, in *Molecular Gels: Materials with Self-Assembled Fibrillar Networks*, ed. R. G. Weiss and P. Terech, Springer, Dordrecht, 2006, pp. 857–893.

39 D. D. Díaz, D. Kühbeck and R. J. Koopmans, *Chem. Soc. Rev.*, 2011, **40**, 427.

40 T. Tanaka, *Sci. Am.*, 1981, **244**, 110.

41 *Polymer Gels: Fundamentals and Biomedical Applications*, ed. D. DeRossi, Y. Kajiwara, Y. Osada and A. Yamauchi, Plenum Press, New York, 1991.

42 S.-K. Ahn, R. M. Kasi, S.-C. Kim, N. Sharma and Y. Zhou, *Soft Matter*, 2008, **4**, 1151.

43 L. A. Estroff and A. D. Hamilton, *Chem. Rev.*, 2004, **104**, 1201.

44 P. Xie and R. Zhang, *J. Mater. Chem.*, 2005, **15**, 2529.

45 A. Ajayaghosh, V. K. Praveen and C. Vijayakumar, *Chem. Soc. Rev.*, 2008, **37**, 109.

46 M. George, R. Mathew and R. G. Weiss, *Mol. Gels*, 2006, 449.

47 D. K. Smith, *Chem. Commun.*, 2006, 34.

48 D. J. Adams, *Macromol. Biosci.*, 2011, **11**, 160.

49 A. Dawn, T. Shiraki, S. Haraguchi, S. Tamaru and S. Shinkai, *Chem. – Asian J.*, 2011, **6**, 266.

50 X. Yang, G. Zhang and D. Zhang, *J. Mater. Chem.*, 2012, **22**, 38.

51 F. Ilmain, T. Tanaka and E. Kokufuta, *Nature*, 1991, **349**, 400.

52 *Polymer Gels and Networks*, ed. Y. Osada and A. R. Khokhlov, Marcel Dekker, New York, 2002.

53 *Synthesis, Characterization, and Theory of Polymeric Networks and Gels*, ed. S. M. Aharoni, Plenum Press, New York, 1992.

54 E. R. Zubarev, M. U. Pralle, E. D. Sone and S. I. Stupp, *Adv. Mater.*, 2002, **14**, 198.

55 X. Huang, P. Terech, S. R. Raghavan and R. G. Weiss, *J. Am. Chem. Soc.*, 2005, **127**, 4336.

56 J. H. Shin, M. L. Gardel, L. Mahadeva, P. Matsudaira and D. A. Weitz, *Proc. Natl. Acad. Sci. U. S. A.*, 2004, **101**, 9636.

57 P. Terech, I. Furman and R. G. Weiss, *J. Phys. Chem.*, 1995, **99**, 9558.

58 H. Ihara, M. Takafuji and T. Sakurai, in *Encyclopedia of Nanoscience and Nanotechnology*, ed. H. S. Nalwa, American Scientific, California, CA, 2004, vol. 9, pp. 473–495.

59 *Low Molecular Mass Gelators*, ed. F. Fages, *Top. Curr. Chem.*, Springer-Verlag, Berlin, Heidelberg, vol. 256, 2005.

60 J. V. Alegre-Requena, E. Marqués-López and R. P. Herrera, *RSC Adv.*, 2015, **5**, 33450.

61 H. Jiang, M. W. Paixão, D. Monge and K. A. Jørgensen, *J. Am. Chem. Soc.*, 2010, **132**, 2775.

62 H. Konishi, T. Y. Lam, J. P. Malerich and V. H. Rawal, *Org. Lett.*, 2010, **12**, 2028.

63 Y. Zhao and D. G. Truhlar, *Theor. Chem. Acc.*, 2008, **120**, 215.

64 Y. Zhao and D. G. Truhlar, *J. Chem. Phys.*, 2006, **125**, 194101.

65 A. D. McLean and G. S. Chandler, *J. Chem. Phys.*, 1980, **72**, 5639.

66 K. Remya and C. H. Suresh, *J. Comput. Chem.*, 2013, **34**, 1341.

67 S. Miertus, E. Scrocco and J. Tomasi, *Chem. Phys.*, 1981, **55**, 117.

68 S. Miertus and J. Tomasi, *Chem. Phys.*, 1982, **65**, 239.

69 S. F. Boys and F. Bernardi, *Mol. Phys.*, 1970, **19**, 553.

70 M. J. Frisch, G. W. Trucks, H. B. Schlegel, G. E. Scuseria, M. A. Robb, J. R. Cheeseman, G. Scalmani, V. Barone, B. Mennucci, G. A. Petersson, H. Nakatsuji, M. Caricato, X. Li, H. P. Hratchian, A. F. Izmaylov, J. Bloino, G. Zheng, J. L. Sonnenberg, M. Hada, M. Ehara, K. Toyota, R. Fukuda, J. Hasegawa, M. Ishida, T. Nakajima, Y. Honda, O. Kitao, H. Nakai, T. Vreven, J. A. Montgomery Jr, J. E. Peralta, F. Ogliaro, M. Bearpark, J. J. Heyd, E. Brothers, K. N. Kudin, V. N. Staroverov, R. Kobayashi, J. Normand, K. Raghavachari, A. Rendell, J. C. Burant, S. S. Iyengar, J. Tomasi, M. Cossi, N. Rega, J. M. Millam, M. Klene, J. E. Knox, J. B. Cross, V. Bakken, C. Adamo, J. Jaramillo, R. Gomperts, R. E. Stratmann, O. Yazyev, A. J. Austin, R. Cammi, C. Pomelli, J. W. Ochterski, R. L. Martin, K. Morokuma, V. G. Zakrzewski, G. A. Voth, P. Salvador, J. J. Dannenberg, S. Dapprich, A. D. Daniels, O. Farkas, J. B. Foresman, J. V. Ortiz, J. Cioslowski and D. J. Fox, *Gaussian 09, revision A.01*, Gaussian, Inc., Wallingford, CT, 2009.

71 E. Marqués-López, J. V. Alegre-Requena and R. P. Herrera, *EP14382260.9*, 2014.

72 *Encyclopedia of Supramolecular Chemistry*, ed. J. W. Steed and J. L. Atwood, Marcel Dekker, New York, vol. 2, 2004.

73 M. Yamanaka, *J. Inclusion Phenom. Macrocyclic Chem.*, 2013, **77**, 33, and references therein.

74 E.-M. Schön, E. Marqués-López, R. P. Herrera, C. Alemán and D. D. Díaz, *Chem. – Eur. J.*, 2014, **20**, 10720.

75 D. Bardelang, *Soft Matter*, 2009, **5**, 1969.

76 X. Yu, L. Chen, M. Zhang and T. Yi, *Chem. Soc. Rev.*, 2014, **43**, 5346.

77 S. Pan, S. Luo, S. Li, Y. Lai, Y. Geng, B. He and Z. Gu, *Chem. Commun.*, 2013, **49**, 8045.

78 J. M. Malicka, A. Sandeep, F. Monti, E. Bandini, M. Gazzano, C. Ranjith, V. K. Praveen, A. Ajayaghosh and N. Armaroli, *Chem. – Eur. J.*, 2013, **19**, 12991.

79 S. Bhattacharya and Y. Krishnan-Ghosh, *Chem. Commun.*, 2001, 185.

80 V. J. Anderson and H. N. W. Lekkerkerker, *Nature*, 2002, **416**, 811.

81 P. Zhu, X. Yan, Y. Su, Y. Yang and J. Li, *Chem. – Eur. J.*, 2010, **16**, 3176.

82 E.-M. Schön, S. Roelens and D. D. Díaz, *CrystEngComm*, 2015, **17**, 8021, and references therein.

83 B. Roy, P. Bairi and A. K. Nandi, *Soft Matter*, 2012, **8**, 2366.

84 N. M. Dixit and C. F. Zukoski, *Phys. Rev. E: Stat., Nonlinear, Soft Matter Phys.*, 2003, **67**, 061501.

85 D. K. Kumar and J. W. Steed, *Chem. Soc. Rev.*, 2014, **43**, 2080.

86 A. Baral, S. Basak, K. Basu, A. Dehsorkhi, I. W. Hamley and A. Banerjee, *Soft Matter*, 2015, **11**, 4944.

87 A. Kotlewski, B. Norder, W. F. Jager, S. J. Picken and E. Mendes, *Soft Matter*, 2009, **5**, 4905.

88 V. A. Mallia, P. D. Butler, B. Sarkar, K. T. Holman and R. G. Weiss, *J. Am. Chem. Soc.*, 2011, **133**, 15045.

89 X. Yu, Q. Liu, J. Wu, M. Zhang, X. Cao, S. Zhang, Q. Wang, L. Chen and T. Yi, *Chem. – Eur. J.*, 2010, **16**, 9099.

90 H. Sato, E. Nogami, T. Yajima and A. Yamagishi, *RSC Adv.*, 2014, **4**, 1659.

91 L. Frkanec and M. Zinic, *Chem. Commun.*, 2010, 522.

92 V. Caplar, M. Zinic, J.-L. Pozzo, F. Fages, G. Mieden-Gundert and F. Vögtle, *Eur. J. Org. Chem.*, 2004, 4048.

93 R. E. Fischer, B. Tadic-Galeb and P. R. Yoder, *Optical System Design*, McGraw Hill, 2nd edn, 2008.

94 K. Lalitha, Y. S. Prasad, V. Sridharan, C. U. Maheswari, G. John and S. Nagarajan, *RSC Adv.*, 2015, **5**, 77589.

95 P. Kirilov, F. Gauffre, S. Franceschi-Messant, E. Perez and I. Rico-Lattes, *J. Phys. Chem. B*, 2009, **113**, 11101.